Bentonite microstructure and saturation evolution in wetting-drying cycles evaluated using ESEM, MIP and WRC measurements

Manuscript submitted to Géotechnique on 06/10/2017 by:

Haiquan Sun[1]
PhD student

Tel: +420221951556
Email: haiquan.sun@natur.cuni.cz

David Mašín[1] (corresponding author)
Associate Professor

Tel: +420221951552
Email: masin@natur.cuni.cz

Jan Najser[1]
Senior Lecturer

Tel: +420221951555
Email: najser@natur.cuni.cz

Vilém Neděla[2]
Researcher

Tel: +420 541 514 333
Email: vilem@isibrno.cz

Eva Navratilova[2]
Researcher

Tel: +420 541 514 333
Email: navratilovae@isibrno.cz

[1] Faculty of Science
Charles University in Prague
Albertov 6, 128 43 Praha
Czech Republic

[2] Institute of scientific instruments
The Czech Academy of Sciences
Královopolská 147, 612 64 Brno
Czech Republic

ABSTRACT

In this paper, microstructure of the Czech bentonite B75 was investigated by three methods: Water retention curve (WRC) measurements, mercury intrusion porosimetry (MIP) measurements and environmental scanning electron microscopy (ESEM) investigation. The experiments were performed on samples of various compaction levels (between 1.27 g/cm^3 and 1.90 g/cm^3) and at various suctions (between 3.3 MPa and 290 MPa) along both drying and wetting hydraulic paths. In the ESEM observations, target relative humidities (and thus total suctions) were imposed directly in the ESEM chamber to observe the effect of hydraulic path on the microstructure. Apart from the inter-lamellar pores, which are not accessible to the adopted experimental techniques, two pore families were identified: micropores and macropores. The transition pore size between the micropores and macropores was found to be suction dependent. The microporosity was practically insensitive to compaction and only largest micropores were sensitive to suction. Smaller macropores were sensitive to compaction only, whereas larger macropores were sensitive to both compaction and suction. We observed that during wetting from the as-compacted state the macropores remained completely dry up to very low values of suction, whereas micropores were found to be unsaturated up to the suctions between 10 MPa to 60 MPa. Both macropores and micropores contributed to sample volume changes during drying and wetting. While the microstructural volume change appeared to be reversible, macrostructure exhibited permanent deformation.

Keywords: bentonite; microstructure; MIP; vapour equilibrium method; ESEM

INTRODUCTION

It is now well accepted that compacted bentonite has a structure with two distinct pore systems, denoted as double-structure (Gens and Alonso, 1995; Alonso, 1998; Alonso et al., 2010). This double structure is explicitly considered in many bentonite constitutive models, focusing on its mechanical behaviour (Alonso et al, 1999), hydraulic behaviour (Romero et al., 2011), coupled hydro-mechanical behaviour (Mašín, 2013; Li et al., 2017; Sánchez et al., 2016; Della Vecchia et al., 2013) or hydro-mechanical behaviour considering the effect of temperature change (Mašín, 2017). In these models, inter-play between mechanical, hydraulic and/or thermal response of micropores and macropores is considered and the global response results from the rearrangement of the macrostructural units and the physical-chemical-mechanical interaction of clay minerals and aggregates. In these models, aggregates are often considered as fully saturated and their mechanical response is assumed to be reversible.

In this paper, we focus on investigation of the effect of wetting and drying on bentonite microstructure. Microstructure is investigated using mercury intrusion posorimetry (MIP) and environmental scanning electron microscopy (ESEM) method, which are supplemented by water retention measurements. Bentonite microstructure has been studied by many authors in the past. Microstructure investigation using MIP has been presented, for example, by Monroy et al. (2010), Lloret and Villar (2007), Romero et al. (2011), Simms and Yanful (2001), Cuisinier and Laloui (2004), Cui (2017) and Romero and Simms (2009). Typically, the authors observe bi-modal pore structure consistent with double structure modelling approach. However, in several recent studies, it has been suggested that consideration of two pore families may be oversimplification of the complex bentonite structure. For example, Wang et al. (2014) identified four major pore sizes, which include inaccessible pores (<6 nm), small pores (6 nm-40nm), medium pores (40 nm-2 μm) and large pores (>2 μm) for MX80 bentonite. Přikryl et al. (2010) investigated the hierarchical porosity of the Czech bentonite from Rokle deposit

(similar to the one used in this study). Four pore size categories were identified by the authors by adsorption isotherms and MIP testing, namely inter-lamellar pores (average radius 0.65 nm), mesopores within individual aggregates (with two peaks corresponding to 2 - 2.5 nm and 5 -10 nm), macropores (+mesopores) between aggregates of clay minerals (2 - 63 μm) and coarse pores (>63 μm) between non-clayey particles of sand size. Monroy et al. (2010) considered three classes of pores, nanoporosity (which can't be detected by MIP technique), microporosity and macroporosity for compacted London clay, with delimiting pore size approximately 2 μm. Microporosity was found to substantially depend on suction. Villar et al. (2014) delimit macropores and meso pores by 5 μm for both MX80 and FEBEX bentonite, the non-intruded pores were named micropores. Manca et al. (2016) found 5 μm to be a delimitation of macro and micropores, and the delimitating pore size was found to be independent of density. Hattab et al. (2013) studied the microstructure of natural and remolded sensitive marine sediment by MIP tests, showing that the compaction is predominantly influencing macropores. Seiphoori et al. (2014) investigated the microstructure of MX80 bentonite under wetting-drying cycles by MIP and SEM tests. A clear transition from a bimodal pore structure to a single pore structure was found upon full saturation, similarly to Monroy et al. (2010).

Scanning electron microscopy (SEM) has been widely used in clay science, which can provide information about bentonite microstructure. The samples used for SEM observation must be completely dried and coated with gold. As the drying process affects bentonite structure substantially, it is preferable to adopt more advanced environmental scanning electron microscopy (ESEM), where vapour pressure (and thus total suction) can be controlled directly in the observation chamber. ESEM technique was used by Watt et al. (2000), who presented that the charge-contrast imaging can improve resolution of ESEM image. Komine and Ogata (1999) found that bentonite aggregates swell into macrovoids along wetting paths, the level of macrovoid occlusion being dependent on bentonite content in sand-bentonite mixture. Romero

(1999) observed the highly compacted Boom clay (2 g/cm^3) under relative humidities of 28%, 53%, 71% and 81% in ESEM chamber. Results showed that irreversible aggregate volume change occurred. Montes et al. (2005) investigated MX80 bentonite at four different densities subjected to hydration/dehydration cycles under ESEM observation. Their results have shown that the mechanical compaction influences the clay microstructure. Villar and Lloret (2001) observed the FEBEX bentonite aggregates by ESEM with a relative humidity between 50% and nearly 100% under constant volume. They have shown that the macropore volume has been reduced due to the swelling of aggregates.

The water retention properties of compacted clay/bentonite were related to its microstructure by various authors. Villar (2007) observed that water retention curve was not dependent on relative density for suctions higher than 10 MPa. Similar observations have been obtained by Romero and Vaunat (2000) and Romero et al. (2011), who adopted double structure framework to interpret water retention behaviour. Similar approach has been chosen by Dieudonne et al. (2017), who separately considered adsorbed water in the micropores and capillary water in the macropores. Gatabin et al. (2016) attributed the difference in water retention curves of bentonite measured under confined and unconfined conditions to its microstructure.

In this paper, we focus on study of the Czech compacted Ca-Mg bentonite from Černý vrch deposit, known as B75. Unlike many previous studies, where MIP testing and ESEM imaging is adopted in a qualitative description of bentonite microstructure, we aim to study the results quantitatively. Combination of the methods allows us to draw unexpected conclusions, which are difficult to obtain using individual methods, such as information about the state of saturation of aggregates and macropores, contribution of macroporosity and microporosity to sample deformation and distinction and properties of pore size classes.

MATERIAL

The Czech bentonite B75 extracted from the Cerny vrch deposit (north-western region of the Czech Republic) and commercially supplied in the form of powder, was used in this study. The montmorillonite content was around 60% and water content of the bentonite powder was about 10%. Table 1 lists its physical parameters. The plastic limit, liquid limit and specific gravity of solid are 65%, 229%, and 2.87, respectively. The cation exchange capacity is shown in Table 2. The chemical composition of bentonite B75 is shown in Table 3.

METHODS

The samples used in the tests were prepared from the bentonite powder at its initial water content by uniaxial compaction in the laboratory mould to reach the desired initial dry density (1.27 g/cm^3, 1.60 g/cm^3 and 1.90 g/cm^3). The height of the sample was 10 mm and the diameter was 50 mm.

Table 4 shows test procedures and initial states of samples in the experiments. The compacted samples were split into two parts. One part was directly equilibrated in the desiccator under controlled suction from 3.29 MPa to 286.7 MPa. The other part was first oven dried, thus reaching approximate suction of 1000 MPa (Nowamooz and Masrouri 2010).

The samples were then either directly equilibrated in desiccator at various suctions for wetting path or equilibrated at the suction of 3.29 MPa and then moved to the higher suction desiccator for WRC measurements along drying paths. Both the sample types, that is samples directly equilibrated at the suctions of 3.29 MPa, 38 MPa and 286.7 MPa and the samples initially oven dried and then equilibrated were used for MIP tests. The samples initially oven dried and then equilibrated at 286.7MPa were used in ESEM observations in variable relative humidity chamber.

The water retention curves were measured at three different initial dry densities (1.27 g/cm^3, 1.60 g/cm^3 and 1.90 g/cm^3), while the ESEM and MIP tests were performed at low (1.27 g/cm^3) and high (1.90 g/cm^3) compaction dry densities only.

Water retention curves

The vapour equilibrium method (Delage et al. 1998) was applied to suction control. Relative humidity in the closed desiccator was controlled by different saturated salt solutions (adopted from OIML,1996). The total suction has a unique relationship with relative humidity described by Kelvin's equation.

$$S_t = \left(\frac{RT\rho_w}{\omega}\right)\ln(1/RH) \qquad (1)$$

Where S_t is the total suction (kPa); R is the molar gas constant, which equals to 8.314462 $J/(mol\ K)$; T is the absolute temperature (K); ρ_w is the density of water (kg/m^3); ω is the molecular mass of water vapour, which equals to 18.016 g/mol ; RH is relative humidity of the system which is defined as the ratio of partial pressure of vapour over saturation vapour pressure.

The relative humidity, solubility and total suction of each saturated salt solution applied in this paper are listed in Table 5. The samples of different dry densities were dried in the oven at 105 °C for over 24 hours. Then, the samples were broken into small irregular pieces weighing between 0.8 and 1.5 g and put into the desiccator. All the desiccators were placed in the air-conditioned room at 20 °C. The samples were not confined, they could thus freely expand during wetting. The weight of the bentonite was regularly measured until the sample mass stabilized. It usually took about 2 months to reach equilibrium, consistently with Tang (2005) (see example results in Figure 1). Once the equilibrium was reached, one part of the samples was used for the equilibrium water content determination, another part was immediately weighted and then covered by wax. The volume was measured using the wax immersion

method following ASTM C914 - 95 (2004) procedure. Water content and void ratio of each of the samples were determined and degree of saturation was calculated from the obtained values.

In order to evaluate the precision of volume measurements using the wax immersion method, three iron balls of different diameter with known volumes were used to calibrate the volume measurements. Figure 2a shows volume errors with respect to measurement number for three different iron ball volumes. Figure 2b shows the relationship between the error and iron ball volume. It can be seen that, as expected, the error increased with decreasing volume. Considering the volume of bentonite used for evaluation of water retention curves, the uncertainty of volume measurements of -5.8% to 7.1% was assumed for calculated void ratio and these values are included as error bars in the graphs presenting the measurement data.

Mercury intrusion porosimetry

Mercury intrusion porosimetry (MIP) is based on the capillary law governing non-wetting liquid (with contact angle bigger than 90°) penetration into small pores. The pore entrance diameter (D) can be determined from the applied mercury pressure (P) by assuming that the cylindrical pores existed in soil according to Washburn equation (Juang and Holtz, 1986):

$$D = -(4\sigma_{Hg}\cos\theta_{nw})/P \quad (2)$$

Where D is the entrance pore diameter, σ_{Hg} is the surface tension of mercury, θ_{nw} is the contact angle between the mercury and soil surface and P is the intrusion pressure. In this study, θ_{nw} =130° and σ_{Hg} =0.484 N/m at 25 °C were considered in pore diameter calculation.

The tests were performed at the Department of Inorganic Technology at the University of Chemistry and Technology Prague (Apparatus Autopore IV, Micromeritics). The measurement was done in two regimes, one is the low pressure regime from 0.01 MPa to 0.2 MPa

(corresponding the pore radius between 100 μm and 3 μm); another one is the high pressure regime from 0.2 MPa to 400 MPa (corresponding the pore radius between 3 μm to 1.5 nm). MIP tests were conducted on freeze dried samples to retain the original microstructure. In freeze drying methods, the samples were firstly immersed into the liquid nitrogen and then the frozen samples were placed under deep vacuum. Finally, the samples went through sublimation in the vacuumed chamber of a freeze dryer.

In the tests, the samples of two different initial dry densities of the as-compacted initial water content were oven dried and then equilibrated at suctions of 286.7 MPa, 38 MPa and 3.29 MPa. Other experiments have been performed on samples with as-compacted initial water content, again equilibrated at the three suction levels of 286.7 MPa, 38 MPa and 3.29 MPa subsequently.

Environmental scanning electron microscopy

The Environmental Scanning Electron Microscopy (ESEM) tests have been performed using QUANTA 650 FEG scanning electron microscope at the Institute of Scientific Instruments of the Czech Academy of Sciences, Brno. The oven dried samples equilibrated at the suction of 286.7 MPa were used for ESEM observations. The samples taken from the desiccator have immediately been prepared for the ESEM test. No cutting tool was used to prepare sample surface; instead, following the procedures of Lin and Cerato (2014), specimen was fractured in order to expose fresh undisturbed section of the sample. The tests were performed at constant temperature of 5°C, the water vapour pressure was imposed directly in the ESEM chamber, which allowed us to observe directly the microstructure response to suction changes. The water vapour pressure of 93 Pa (relative humidity of 10%, suction of 290.75 MPa) was determined as optimal initial state for the experiment. Then the vapour pressure was gradually increased up to 850 Pa (relative humidity 97%, suction of 3.85 MPa). After relative humidity reached its maximum value, it was gradually decreased back to 10%. The test conditions are summarized

in Table 6. The interval between vapour pressure changes was 15 minutes. Similar interval was adopted by other researchers (Montes-H, 2005 and Lin and Cerato 2014).

RESULTS AND DISCUSSION

The effect of oven drying on microstructure

As some samples (see Table 4) used for WRC, ESEM and MIP measurements were first oven-dried at 105 °C before testing and the temperature could potentially affect their microstructure, we evaluated this effect first. Figure 3 shows pore size density curves measured by MIP method of samples compacted to dry densities 1.27 g/cm^3 and 1.90 g/cm^3 directly equilibrated at the suction of 38 MPa compared with MIP results of the samples equilibrated at the same suction after oven drying. The effect of oven drying on MIP curves is insignificant, apart of its effect on the largest pores, where it can be attributed to mechanical hysteresis due to drying-wetting cycle. We thus consider the effect of oven drying to not affect qualitative and quantitative evaluation of presented data.

Water retention curves

Figure 4a shows the water retention curves of samples at three initial dry densities (wetting and drying path). It is clear that the initial dry density had only little influence on water content. With the assumption that most water is concentrated in the micropores at high suctions, these results suggest that micropores are only little influenced by the compaction pressures as if their volume would be affected, also their water retention capacity (which is known to be porosity-dependent) would change. Contrary, quite a remarkable effect of the initial dry density was found on degree of saturation (Figure 4d,e) through its effect on void ratio (Figure 4b,c). Although the void ratio measurements using the wax immersion method are subjected to an

error (indicated as shaded areas in Figure 4b to Figure 4e), the measurements consistently show an increase in the global degree of saturation with increasing dry density.

Mercury intrusion porosimetry measurements

Figure 5 shows the MIP results of low (1.27 g/cm^3) and high (1.90 g/cm^3) density samples at each suction level. Figure 6 then shows the same results, replotted to identify the effect of suction on pore size density curves. The MIP data allow us to identify the effects of suction and compaction level on the individual pore sizes. Apart of the inter-lamellar pores, which are not accessible to the adopted measurement techniques, we can distinguish two primary pore size domains:

1. "Micropores": between 3nm and micro-macro transition pore radius. Micropores are defined with the aid of Figure 5 and Figure 6 as smaller pores which are practically unaffected by compaction. The transition pore radii were identified on high density samples as the maximum pore size which remained open after compaction (in low density samples, the transition pore radius was not clear due to the dominant effect of macropores). The obtained transition pore radii were 0.07 μm, 0.15 μm and 0.3 μm for suctions of 286.7 MPa, 38MPa and 3.29 MPa respectively.
2. "Macropores", which are larger than the micro-macro transition pore radius. This is a family of larger pores, which are affected by compaction level.

More detailed study of Figures 5 and 6 reveals that in both the two pore families, only the larger pores are affected by suction: above 0.025 μm for micropores and and above 2.5 μm for macropores. It thus seems that, at each level of structure, larger pores are more deformable and are thus more responsive to change in suction forces. In Figure 7, void ratios corresponding to the individual pore sizes are quantified from the cumulative pore size distribution curves. It is clear that the compaction level influences mainly the macropores, following the definition

which we adopted for distinction of transition pore radius. Micropores are relatively insensitive to compaction effort and they are moderately sensitive to suction, while only the largest micropores contribute to deformation due to suction change. Finally, in Figure 8, cumulative pore size density functions obtained in MIP measurements are compared with void ratios obtained from wax immersion measurement method (results of wax immersion measurements are plotted along with the error range). Both the measurement methods are subjected to inaccuracies; errors in wax immersion method of volume measurement have already been discussed. In addition, MIP evaluation is based on an assumption of cylindrical pore size. Irrespectively of these assumptions, however, it appears that both measurements are relatively consistent with each other in low initial dry density samples. In high initial dry density samples, void ratios extracted from MIP data are lower than the wax immersion method measured void ratios, but relative positions of the curves for different suctions are consistent between the two methods.

Environmental scanning electron microscopy observations

Figure 9 shows example ESEM micrographs of the compacted bentonite with a dry density of 1.27 g/cm^3 which was equilibrated at the total suction of 286.7 MPa. The arrangement of aggregates may clearly be seen, along with different pore families. The aggregates are clearly visible at lower magnification (complete photo and Zoom 1), Zoom 2 and Zoom 3 then show details of the aggregate structure with microporosity. The micrographs of compacted bentonite subjected to wetting and drying in the ESEM chamber are presented in Figure 10 for dry density of 1.27 g/cm^3 and in Figure 11 for dry density of 1.90 g/cm^3. These photos are qualitatively consistent with MIP observations: macropores and distinct aggregates are visible at low dry density sample, only aggregates with fine bentonite matrix, without clear macroporosity, are visible at high dry density samples. It is also clear that macropores remain dry at most suction levels, apart of lowest suction at high dry density soil (Figure 11c), where water menisci in

macropores start to be identifiable in the photos. Water retention measurements (in particular, independence of water content on compaction level, Figure 4a) are consistent with these observations.

To quantitatively analyse the measured data, we evaluated macroporosity evolution with suction and aggregate size variation with suction. To identify macroporosity evolution with suction, we have included double arrow in Figure 10 and Figure 11, which is indicating the distance between the selected aggregates. The macropore size increases upon wetting and decreases upon drying, consistently with MIP data, which have shown suction dependency of the larger macropores. We could also observe hysteretic phenomenon occuring after one wetting-drying cycle. The aggregate distance was larger after wetting-drying cycle than initially. Recall that, consistently with these measurements, oven drying-wetting cycle on low density samples caused smaller volume of larger macropores compared to directly equilibrated samples (Figure 3). Wetting-drying cycle thus caused macroporosity opening, whereas drying-wetting cycle caused its densification.

In order to quantitatively analyse the volume change of aggregates upon wetting and drying, the digital image analysis technique was used. The original ESEM photo represents a plan view in two-dimensions, as shown in Figure 12a. Firstly, the original ESEM photos were adjusted by threshold grey level to clearly identify the boundary of the aggregates. Then, the surface area of the aggregate was measured using a software tool at each stage (see Figure 12b to Figure 12d). Once the surface area was obtained, appropriate aggregate volume was calculated based on assumption of its spherical shape. We set the first observation at the suction of 290.75 MPa as a starting point. Then, the volume strain can be calculated. The volume strain is used to define the relative volume change of the aggregate, defined as

$$\varepsilon_V = (V_i - V_0)/(V_0) \qquad (4)$$

where ε_v is the volume strain, V_i is the volume of the aggregate at the stage i, V_0 is the volume of the aggregate at the initial state.

We chose four different aggregates of each dry density to analyse their volume strain with suction. Figure 13 and Figure 14 show the selected aggregates from ESEM photos of low and high density samples. The volume strain upon wetting and drying paths is shown in Figure 15. The volume strain increased with decreasing suction, however, this increase was relatively minor up to the low suction of 3.3 MPa. At this suction, we can see a sudden increase in volume strain, but we presume the values are affected by water entering the macropores which caused the aggregate boundaries to be less clearly defined at the photomicrograph. During drying, water remained initially in the macropores due to hydraulic hysteresis and thus also the apparent aggregate volume was affected. Above suction of 38.02 MPa, however, only very small effect of hydraulic hysteresis is measured: aggregate volumetric response thus appears to be reversible with suction.

Evaluation of aggregate saturation

Based on the volumetric strain of selected aggregates and water content determined from water retention curves, calculation of the aggregate saturation was carried out. The aggregate saturation was investigated along wetting path (for both ESEM and WRC measurements), because it was not affected by presence of inter aggregate water up to very low suctions. The calculation of aggregate saturation comprised the following steps:

- Water content corresponding to each suction applied in ESEM chamber was calculated by interpolation from wetting path of water retention curves. For all studied aggregates, the suctions just before water entered macropores was considered as a threshold state, in which aggregates were fully saturated, but inter-aggregate pores were dry. This state

corresponded to 3.85 MPa for low density samples and 7.8 MPa for high density samples.

- Volume of micropores was then calculated with the assumption of full saturation of aggregates from the water content at the threshold state. At this state, the calculated S_r was equal to one by definition (see Figure 16).
- Subsequently, the volume change of the aggregates for each higher suction was calculated from ESEM microphotograph analysis (Figure 15). Corresponding water content for each particular suction was interpolated from water retention curve. Based on these values, degree of saturation could be calculated for each aggregate and each suction along the wetting path.

Despite the adopted assumptions adopted in volume strain estimation, including full saturation of microstructure at water-expulsion value of suction, dry inter aggregate space and spherical shape of the aggregates, the calculation of S_r for all 8 aggregates gives relatively consistent results (Figure 16). It indicates that during wetting the samples were unsaturated down to the values of suction between 10 MPa and 60 MPa, the air expulsion value of suction being higher at high dry density samples. These values are lower compared to the assumption of fully saturated aggregates up to the suctions of 80-100 MPa (Delage et al, 1998, Mašín and Khalili, 2015).

CONCLUDING REMARKS

In the paper, we presented results of water retention measurements along with void ratio measurements, MIP tests and ESEM micrographs of the Czech B75 Ca-Mg bentonite at various initial dry densities. Results of the methods were quantitatively analysed and compared, leading to the following main conclusions:

- Apart from the inter-lamellar pores, which are not accessible to the adopted observation methods, we could identify two main pore families. Their transition pore size was suction-dependent (0.07 μm to 0.3 μm for suctions varying between 286.7 MPa and 3.29 MPa). The micropores was practically insensitive to compaction and only largest micropores were sensitive to suction. The smaller macropores were sensitive to compaction only, whereas the larger macropores were sensitive to both compaction and suction.
- During wetting from the as-compacted state the macroporosity remained completely dry up to very low values of suction (3.29 MPa).
- During wetting from the as-compacted state the micropores were found to be unsaturated up to the suction values between 10 MPa to 60 MPa.
- Both macropores and micropores contributed to sample volume changes during suction change. While the micropore volume change appeared to be reversible, permanent deformation remained on the macropore level. Wetting-drying cycle caused macroporosity loosening, whereas oven drying-wetting cycle caused densification of the largest macropores.
- Oven drying at 105 °C and subsequent wetting was found to have little effect on bentonite microstructure, apart of its effect on the largest macropores, where it may be attributed to the mechanical hysteresis effects, however.

ACKNOWLEDGEMENTS

This project receives funding from the Euratom research and training programme 2014-2018 under grant agreement No 745942. The first author acknowledges support by the grant No. 846216 of the Charles University Grant Agency. Institutional support by Center for Geosphere Dynamics (UNCE/SCI/006) is greatly appreciated. Dr. Sedlářová of the University of

Chemistry and Technology (Prague) and Dr. Plachý of the Czech Agriculture University are acknowledged MIP testing and sample preparation respectively.

NOTATION - List of symbols

I_p Plasticity index

ρ_s Particle density

w_c Water content

S_r Degree of saturation

e Void ratio

e_0 Initial void ratio

S_t Total suction

R Molar gas constant

T Absolute temperature

ρ_w Density of water

ω Molecular mass of water vapour

RH Relative humidity

D Entrance pore diameter

σ_{Hg} Surface tension of mercury

θ_{nw} Contact angle between the mercury and soil surface

P Intrusion pressure

ε_v Volume strain

V_i Volume of the aggregate at the stage i

V_0 Volume of the aggregate at the initial state

REFERENCES

Alonso, E.E., Vaunat, J., Gens, A. (1999). Modelling the mechanical behaviour of expansive clays. Engineering Geology 54, 173–183.

Alonso, E. E., Pereira, J. M., Vaunat, J., & Olivella, S. (2010). A microstructurally based effective stress for unsaturated soils. Géotechnique, 60(12), 913-925.

Beckett, C.T. and Augarde, C.E., (2013). Prediction of soil water retention properties using pore-size distribution and porosity. Canadian Geotechnical Journal, 50(4), pp.435-450.

Cuisinier, O., Laloui, L. (2004). Fabric evolution during hydromechanical loading of a compacted silt. Canadian Geotechnical Journal 28, 483–499.

Cui, Y.-J. (2017). On the hydro-mechanical behaviour of MX80 bentonite-based materials. Journal of Rock Mechanics and Geotechnical Engineering 9, 565-574.

Delage, P., Audiguier, M., Cui, Y. J. and Howat, M. D. (1996). Microstructure of a compacted silt. Canadian Geotechnical Journal. 33, 150-158

Delage, P., M. D. Howat, and Y. J. Cui (1998). The relationship between suction and swelling properties in a heavily compacted unsaturated clay. Engineering Geology 50, 31–48.

Della Vecchia, G., Jommi, C., Romero, E. (2013). A fully coupled elastic–plastic hydrome-chanical model for compacted soils accounting for clay activity. Int. J. Numer. Anal. Methods Geomech. 37 (5), 503–535.

Dieudonne, A. C., Della Vecchia, G., & Charlier, R. (2017). Water retention model for compacted bentonites. Canadian Geotechnical Journal, 54(7), 915-925.

Gatabin, C., Talandier, J., Collin, F., Charlier, R., & Dieudonné, A. C. (2016). Competing effects of volume change and water uptake on the water retention behaviour of a compacted MX-80 bentonite/sand mixture. Applied Clay Science, 121, 57-62.

Gens, A. and Alonso, E. E. (1992). A framework for the behaviour of unsaturated clays. Canadian Geotechnical Journal. 29, 1013-1032

Hattab, M., Hammad, T., Fleureau, J. M., & Hicher, P. Y. (2013). Behaviour of a sensitive marine sediment: microstructural investigation. Géotechnique, 63(1), 71-84.

Hausmannova. L and Vasicek. R, (2014). Measuring hydraulic conductivity and swelling pressure under high hydraulic gradients. Geological Society, London, Special Publications, v.400; p293-301. doi: 10.1144/SP400.36

Komine H, Ogata N (1999). Experimental study on swelling characteristics of sand–bentonite mixture for nuclear waste disposal. Soils Found 39(2):83–97

Li, J., Yin, Z.-Y., Cui, Y., Hicher, P.-Y. (2017). Work input analysis for soils with double porosity and application to the hydromechanical modeling of unsaturated expansive clays. Canadian Geotechnical Journal 54 (2), pp. 173-187.

Lin, B., & Cerato, A. B. (2014). Applications of SEM and ESEM in Microstructural Investigation of Shale-Weathered Expansive Soils along Swelling-Shrinkage Cycles. Engineering Geology, 177, 66-74.

Lloret A., Villar M.V., Sánchez M., Gens A., Pintado X., Alonso E.E. (2003). Mechanical behaviour of heavily compacted bentonite under high suction changes. Géotechnique, 53 (1), pp. 27–40

Lloret, A., Villar,M.V. (2007). Advances on the knowledge of the thermo-hydro-mechanical behaviour of heavily compacted “FEBEX” bentonite. Physics and Chemistry of the Earth 32, 701–715.

Manca, D., Ferrari, A., & Laloui, L. (2016). Fabric evolution and the related swelling behaviour of a sand/bentonite mixture upon hydro-chemo-mechanical loadings. Géotechnique, 66(1), 41-57.

Mašín D. (2013). Double structure hydromechanical coupling formalism and a model for unsaturated expansive clays. Engineering Geology; 165:73–88.

Mašín D. (2017). Coupled Thermohydromechanical Double-Structure Model for Expansive Soils. ASCE Journal of Engineering Mechanics, 143(9), 04017067.

Mašín, D., & Khalili, N. (2015). Swelling phenomena and effective stress in compacted expansive clays. Canadian Geotechnical Journal, 53(1), 134-147.

Monroy, R., Zdravkovic, L., Ridley, A. (2010). Evolution of microstructure in compacted London Clay during wetting and loading. Geotechnique 60 (2), 105–119.

Montes-H, G. (2005). Swelling–shrinkage measurements of bentonite using coupled environmental scanning electron microscopy and digital image analysis. Journal of colloid and interface science, 284(1), 271-277.

Montes-H, G., Geraud, Y., Duplay, J., & Reuschle, T. (2005). ESEM observations of compacted bentonite submitted to hydration/dehydration conditions. Colloids and Surfaces A: Physicochemical and Engineering Aspects, 262(1-3), 14-22.

Nowamooz, H., & Masrouri, F. (2010). Relationships between soil fabric and suction cycles in compacted swelling soils. Engineering geology, 114(3), 444-455.

Přikryl, R., & Weishauptová, Z. (2010). Hierarchical porosity of bentonite-based buffer and its modification due to increased temperature and hydration. Applied Clay Science, 47(1-2), 163-170.

Push R. (1982). Mineral-water interactions and their influence on the physical behavior of highly compacted Na-bentonite. Canadian Geotechnical Journal, 19 (3): 381–387.

Romero E (1999). Characterisation and thermo-hydro- mechanical behaviour of unsaturated Boom-clay: An experimental study. Ph. D. Thesis, Universitat Politecnica de Catalunya, Barcelona.

Romero E. and Vaunat J. (2000). Retention curves of deformable clays. A. Tarantino, C. Mancuso (Eds.), Experimental evidence and theoretical approaches in unsaturated soils. Proceedings of an international workshop on unsaturated soils, A.A. Balkema, Rotterdam, Netherlands, pp. 91–106

Romero, E. and Simms, P. H. (2008). Microstructure investigation in unsaturated soils: A re-view with special attention to contribution of mercury intrusion porosimetry and environmental scanning electron microscopy. Geotechnical and Geological Engi- neering 26, 705–727.

Romero, E., Gens, A., & Lloret, A. (1999). Water permeability, water retention and microstructure of unsaturated compacted Boom clay. Engineering Geology, 54(1), 117-127.

Romero, E., Della Vecchia, G., Jommi, C. (2011). An insight into the water retention prop-erties of compacted clayey soils. Geotechnique 61 (4), 313–328.

Saba, S., Delage, P., Lenoir, N., Cui, Y. J., Tang, A. M., & Barnichon, J. D. (2014). Further insight into the microstructure of compacted bentonite–sand mixture. Engineering geology, 168, 141-148.

Sánchez, M., Gens, A., Villar, M.V., Olivella, S. (2016). Fully coupled thermo-hydro-mechanical double-porosity formulation for unsaturated soils. International Journal of Geomechanics 16 (6), D4016015.

Seiphoori, A., Ferrari, A., & Laloui, L. (2014). Water retention behaviour and microstructural evolution of MX-80 bentonite during wetting and drying cycles. Géotechnique, 64(9), 721-734.

Simms, P.H., Yanful, E.K., 2001. Measurement and estimation of pore shrinkage and pore distribution in a clayey till during soil–water-characteristic curve tests. Canadian Geotechnical Journal 38, 741–754.

Simms, P. H., & Yanful, E. K. (2005). A pore-network model for hydromechanical coupling in unsaturated compacted clayey soils. Canadian Geotechnical Journal, 42(2), 499-514.

Stastka, J. and Smutek, J. (2015). Experimental works with bentonite pellets at the CEG. LUCOEX Conference and workshop – Full-scale demonstration tests in technology development of repositories for disposal of radioactive waste. Oskarshamn, Sweden. pp. 179-184

Sun, H., Mašín, D. and Boháč, J. (2017). Experimental characterization of retention properties and microstructure of the Czech bentonite B75. Proc. 19th ICSMGE, Seoul, Korea, 1249-1252.

Tang, A. M., & Cui, Y. J. (2005). Controlling suction by the vapour equilibrium technique at different temperatures and its application in determining the water retention properties of MX80 clay. Canadian Geotechnical Journal, 42(1), 287-296.

The International Organization of Legal Metrology (OIML). (1996). The scale of relative humidity (RH) of air certified against saturated salt solutions. OIMLR 121, France.

Villar, M. V., Gomez-Espina, R., Campos, R., Gutierrez-Nebot, L., & Barrios, I. (2014). Retention curves of bentonite under a microstructural perspective. In Unsaturated Soils (Vol. 2, pp. 989-994). Taylor and Francis - Balkema.

Villar, M. V. (2007). Water retention of two natural compacted bentonites. Clays and Clay Minerals, 55(3), 311-322.

Villar, M. V., & Lloret, A. (2004). Influence of temperature on the hydro-mechanical behaviour of a compacted bentonite. Applied Clay Science, 26(1-4), 337-350.

Villar, M. V., & Lloret, A. (2001). Variation of the intrinsic permeability of expansive clays upon saturation. Clay science for engineering. Balkema, Rotterdam, 259-266.

Wang, Q., Cui, Y.-J., Tang, A. M., Li, X.-L., Ye, W.-M. (2014). Time- and density-dependent microstructure features of compacted bentonite. Soils and Foundations, Vol. 54, No. 4, 657-666.

Watt GR, Griffin BJ, Kinny PD (2000). Charge contrast imaging of geological materials in the environmental scanning electron microscope. Am Miner 85:1784–1794

Table 1: Montmorillonite content and physical properties of bentonite B75 (Stastka et al., 2015)

Property	Description
Montmorillonite (%)	60
Liquid limit (%)	229
Plastic limit (%)	65
Plasticity index Ip	164
Particle density ρs (g/cm^3)	2.87

Table 2: Cation exchange capacity of bentonite B75 (Sun et al., 2017)

Cation	meq/100 g
Ca^{2+}	36.92
Na^{+}	65.75
K^{+}	3.03
Mg^{2+}	26.84
H^{+}	<0.5

Table 3: The chemical composition of bentonite B75 (Hausmannová, 2014)

Component	Weight (%)
SiO_2	51.91
Al_2O_3	15.52
Fe_2O_3	8.89
TiO_2	2.28
CaO	4.6
MgO	2.22
Na_2O	1.21
K_2O	1.27
P_2O_5	0.4
MnO	0.11
FeO	2.95
SO_3	0.09
$CaCO_3$	11.71
CO_2	5.15

Table 4: Test programme

Initial ρ_d	Initial W_C	Initial Suction	Sample state	Suction paths (MPa)
1.27 g/cm^3	10%	48.57 MPa	Oven dried	WRC: 286.7→3.29 MPa ESEM: 290.75→3.85→290.75 MPa MIP : 286.7, 38.00, 3.29 MPa
			Directly equilibrated	MIP : 286.7, 38.00, 3.29 MPa
			Equilibrated at suction of 3.29 MPa	WRC: 3.29→286.7 MPa
1.6 g/cm^3	10%	46.65 MPa	Oven dried	WRC: 286.7→3.29 MPa
			Equilibrated at suction of 3.29 MPa	WRC: 3.29→286.7 MPa
1.9 g/cm^3	10%	49.29 MPa	Oven dried	WRC: 286.7→3.29 MPa ESEM: 290.75→3.85→290.75 MPa MIP: 286.7, 38.00, 3.29 MPa
			Directly equilibrated	MIP : 286.7, 38.00, 3.29 MPa
			Equilibrated at suction of 3.29 MPa	WRC: 3.29→286.7 MPa

Table 5: Salt solutions used for vapour equilibrium method measurements (for temperature of 20 °C) (OIML, 1996)

Salt solutions	Solubility (g/100ml)	Relative humidity (%)	Suction (MPa)
$LiCl \cdot H_2O$	82.78	12.0	286.7
CH_3COOK	268.6	23.1	198.14
$MgCl_2 \cdot 6H_2O$	55.24	33.1	149.51
K_2CO_3	109.43	43.2	113.50
NaBr	91.21	59.1	71.12
NaCl	36	75.5	38.00
KCl	34	85.1	21.82
K_2SO_4	11.05	97.6	3.29

Table 6: Water vapour pressure, relative humidity and total suction adopted in ESEM measurements.

Temperature 5 °C		
Relative humidity (%)	Water vapour pressure (Pa)	Total suction (MPa)
10	93	290.75
30	266	152.03
50	439	87.52
60	519	64.50
74	649	38.02
80	692	28.18
90	785	13.30
97	850	3.85
90	785	13.30
80	692	28.18
74	649	38.02
60	519	64.50
50	439	87.52
30	266	152.03
10	93	290.75

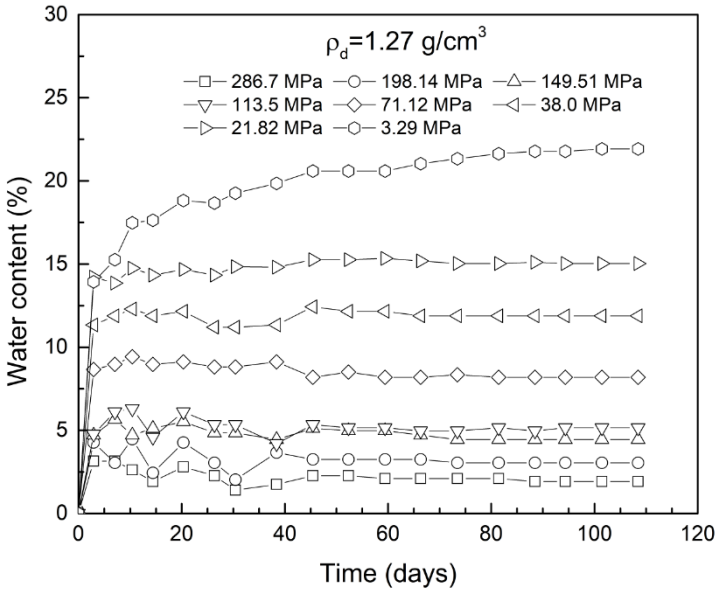

1

2 *Figure 1: Example of water content time evolution in WRC measurements by vapour*
3 *equilibrium method for initial dry density of 1.27 g/cm³.*

4

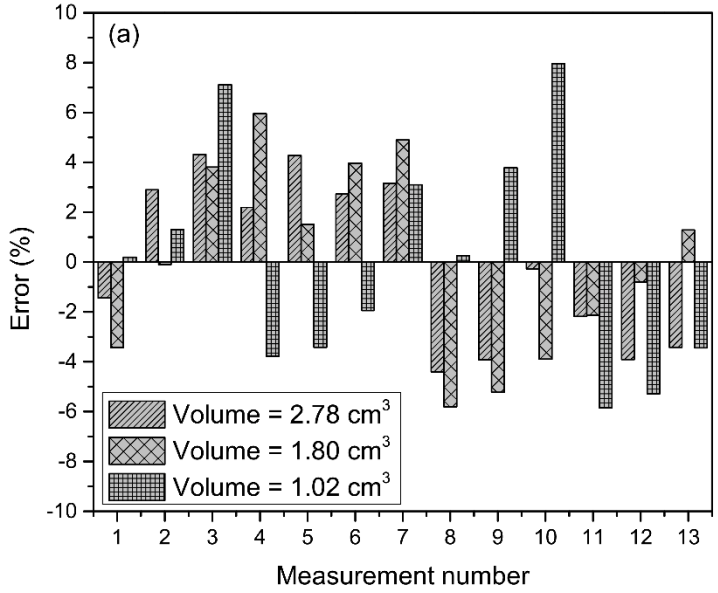

1

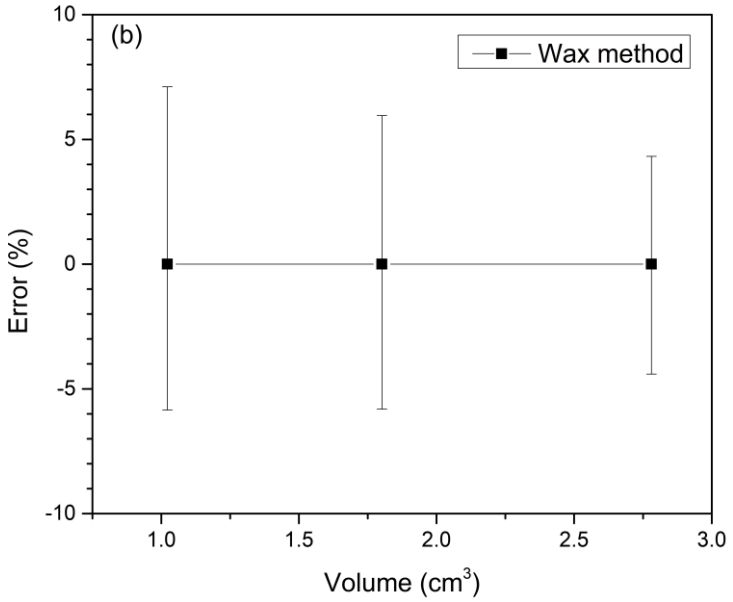

2

3 *Figure 2: Uncertainty of volume measurement by wax immersion method.*

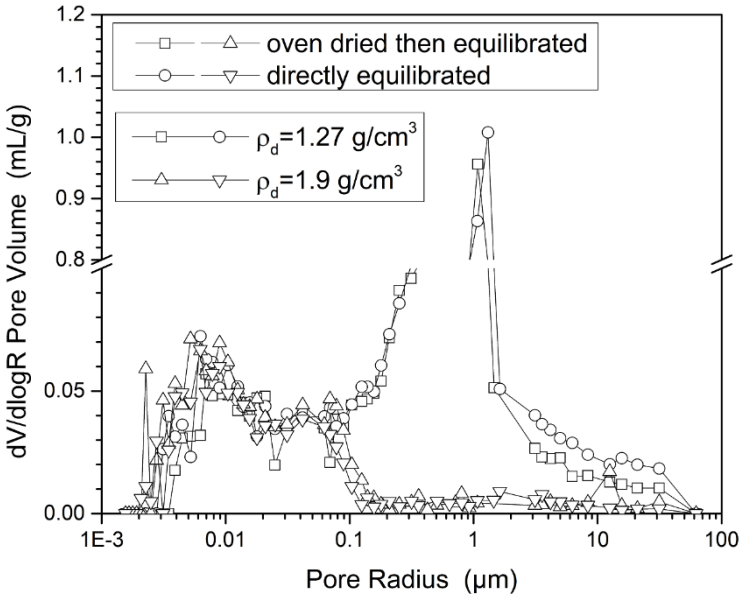

Figure 3: The effect of oven drying on pore size distribution of 1.27 g/cm³ and 1.90 g/cm³ samples.

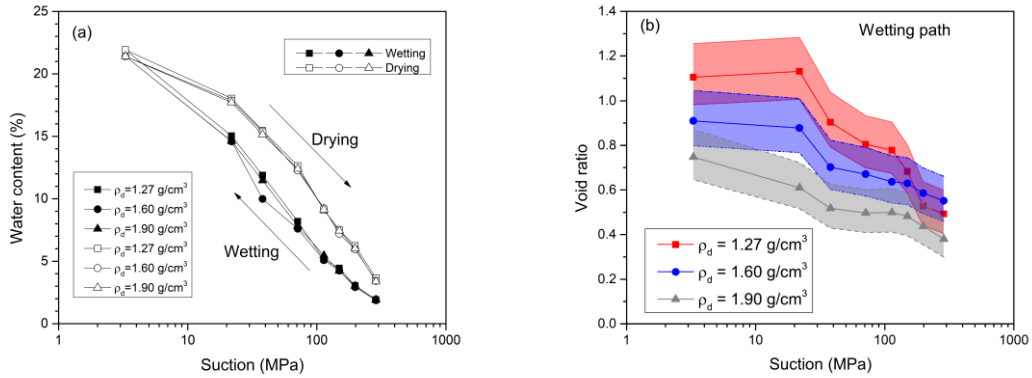

1

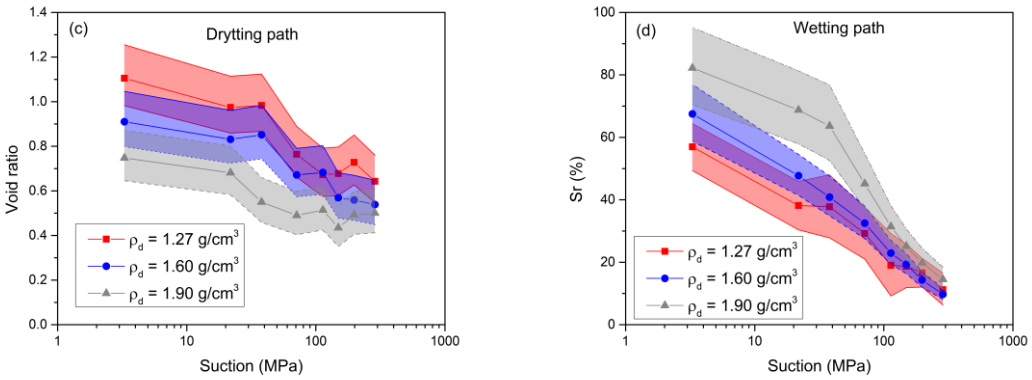

2

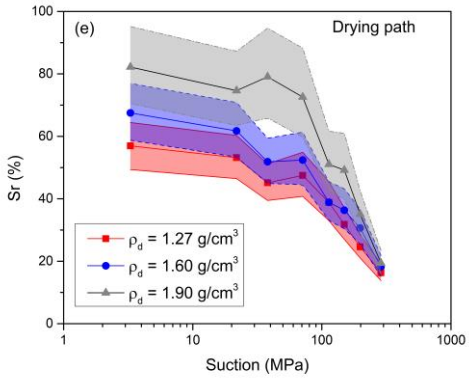

3

4 *Figure 4: Water content, void ratio and degree of saturation with respect to suction for*
5 *water retention curve measurements along wetting and drying path at three different initial*
6 *dry densities.*

7

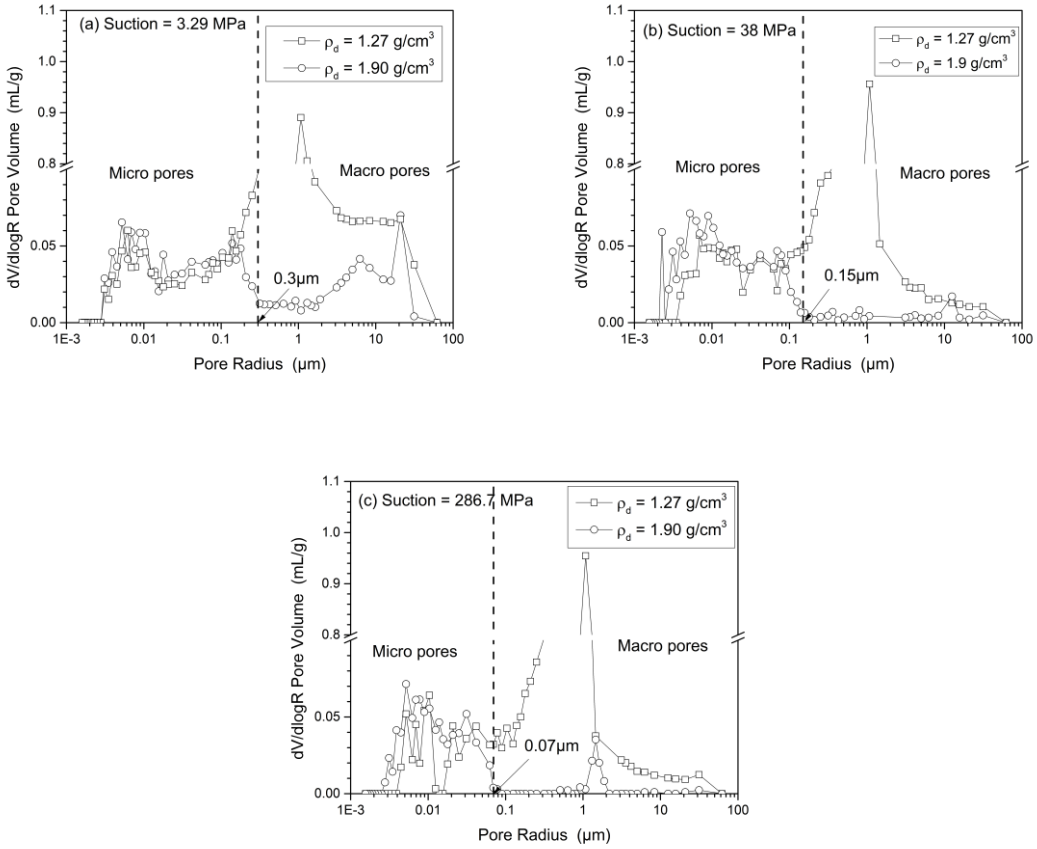

Figure 5: Pore size distribution curves, the effect of dry density.

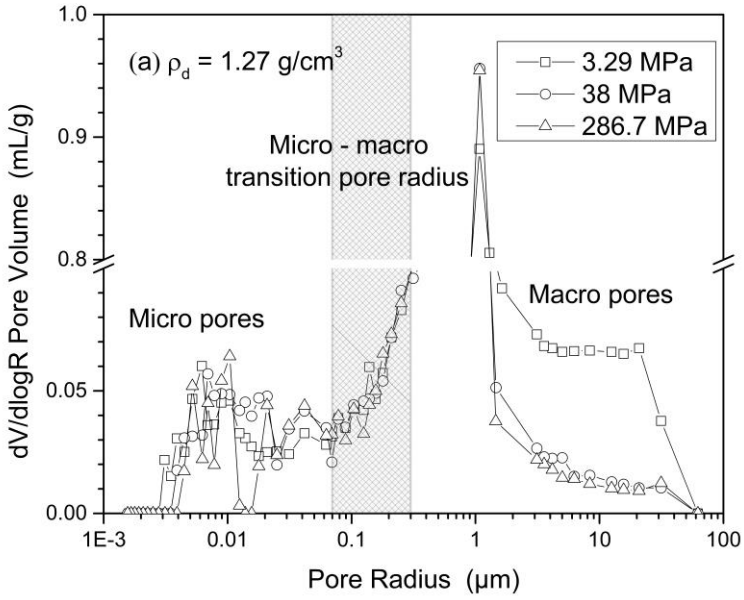

1

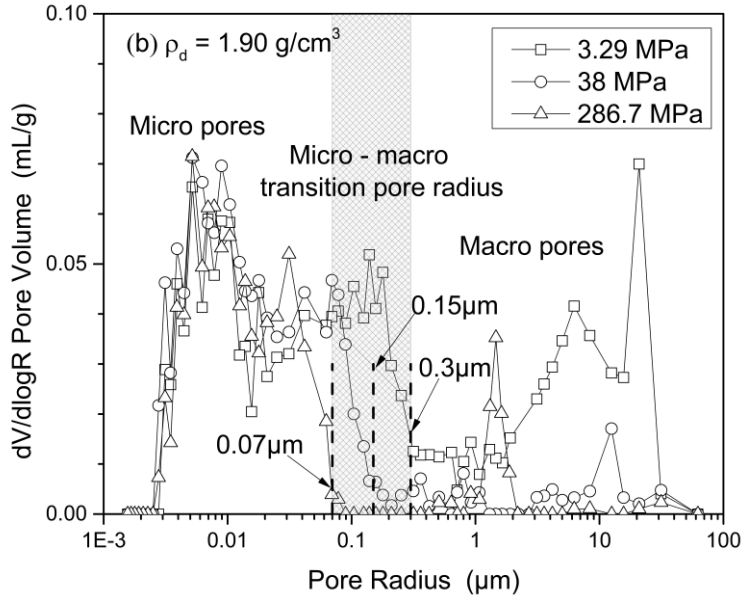

2

3 *Figure 6: Pore size distribution curves, the effect of suction and indication of micro-macro*
4 *transition pore radius.*

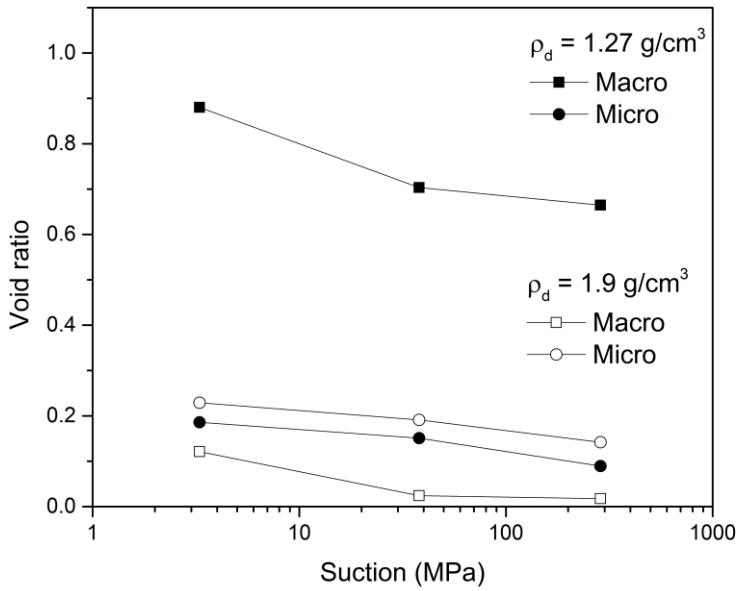

Figure 7: Void ratios corresponding to the individual pore families calculated from MIP data.

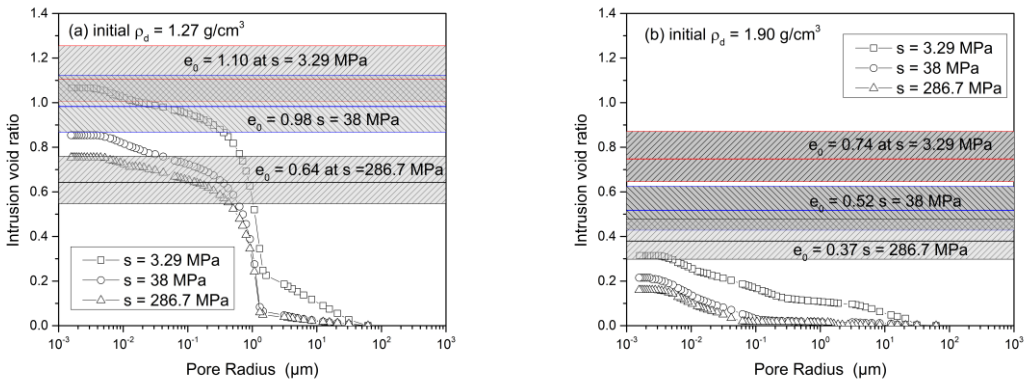

Figure 8: Cumulative pore size distribution curves along with void ratios obtained during WRC measurements.

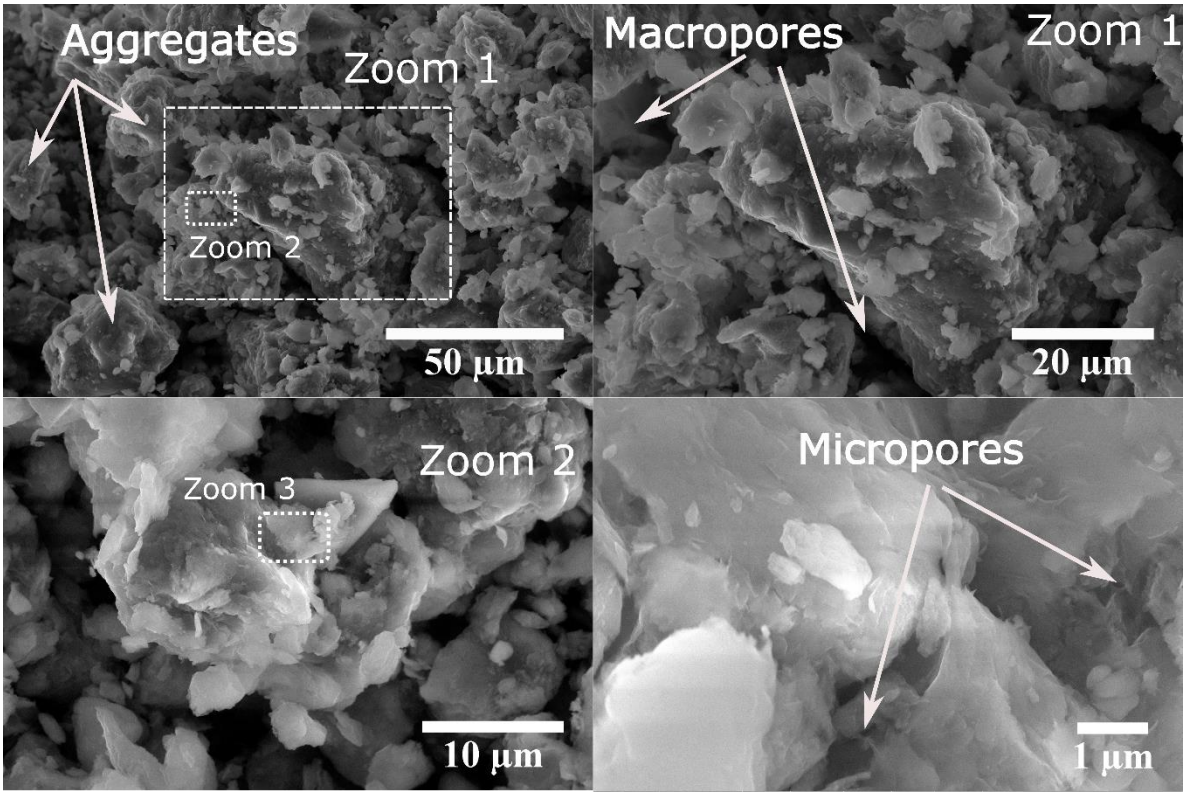

Figure 9: ESEM micrographs of compacted bentonite with a dry density of 1.27 g/cm^3 at different magnifications (note that "Zoom 2" and "Zoom 3" images are from different sample section than the main photo and "Zoom 1" image).

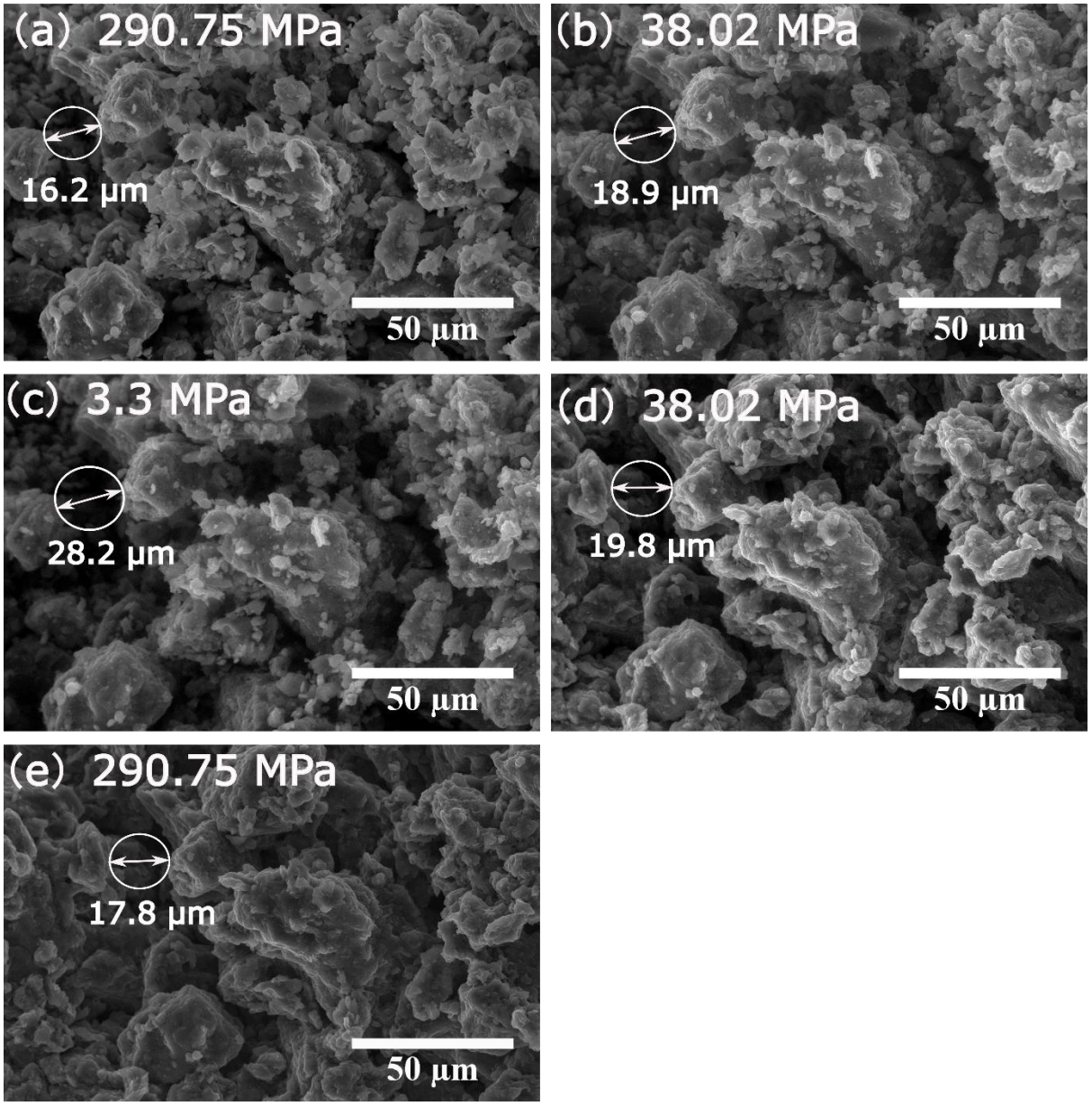

Figure 10: Selected ESEM micrographs of compacted bentonite with a dry density of 1.27 g/cm^3 under the wetting-drying path.

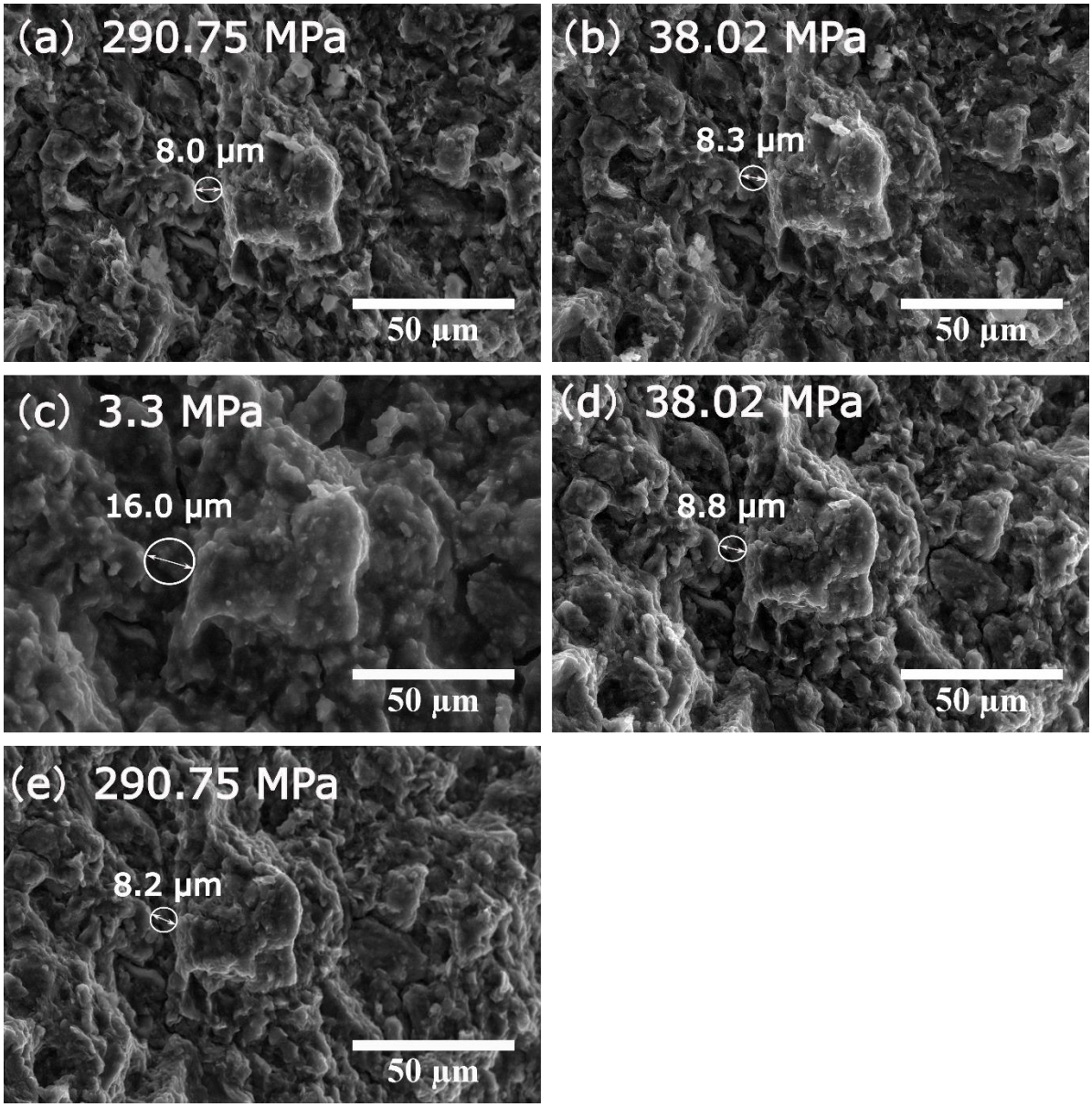

Figure 11: Selected ESEM micrographs of compacted bentonite with a dry density of 1.9 g/cm^3 under the wetting-drying path.

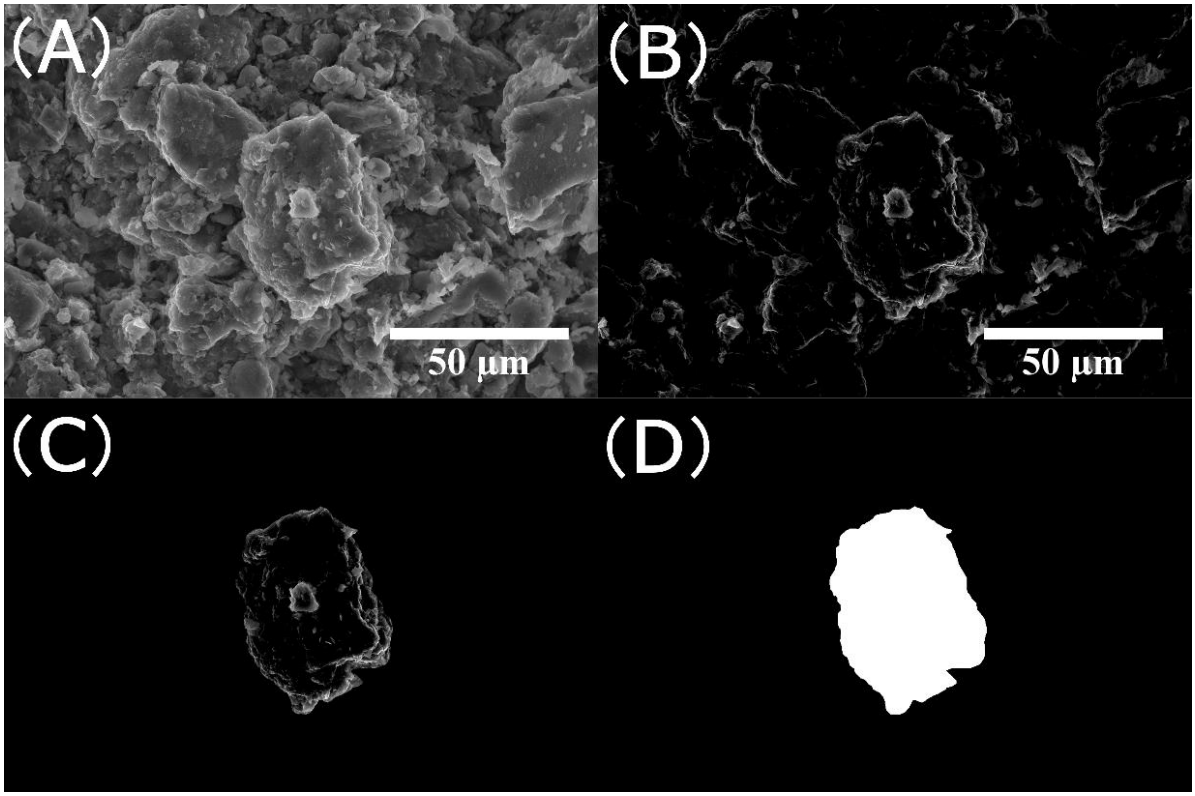

Figure 12: Digital image analysis methodology for target aggregates, (A) original ESEM microphotographs, (B) Image grey level adjustment, (C) target aggregates, (D) measurement of the surface area.

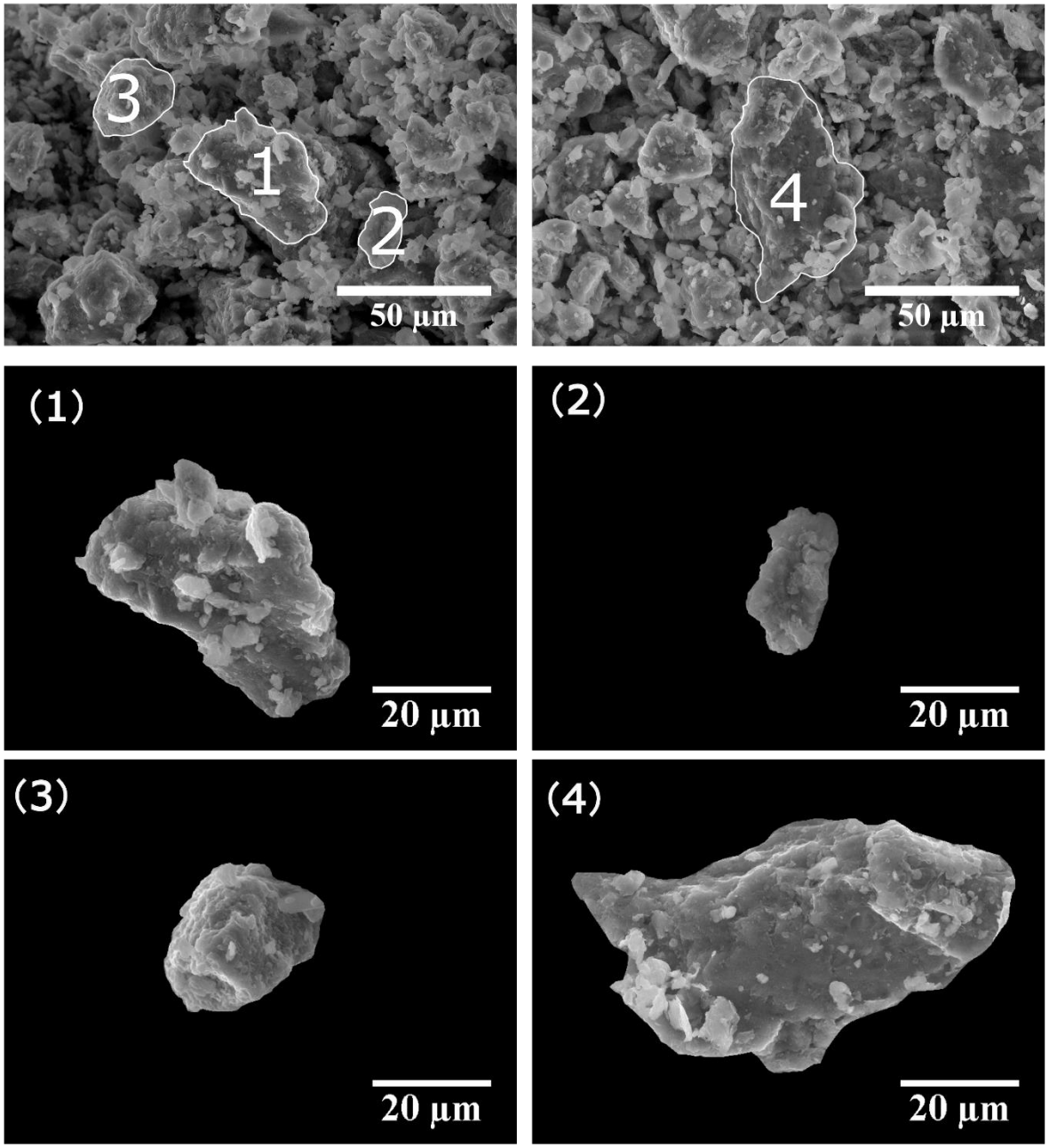

Figure 13: Aggregates of the initial dry density 1.27 g/cm^3 samples selected for calculation of volume strain.

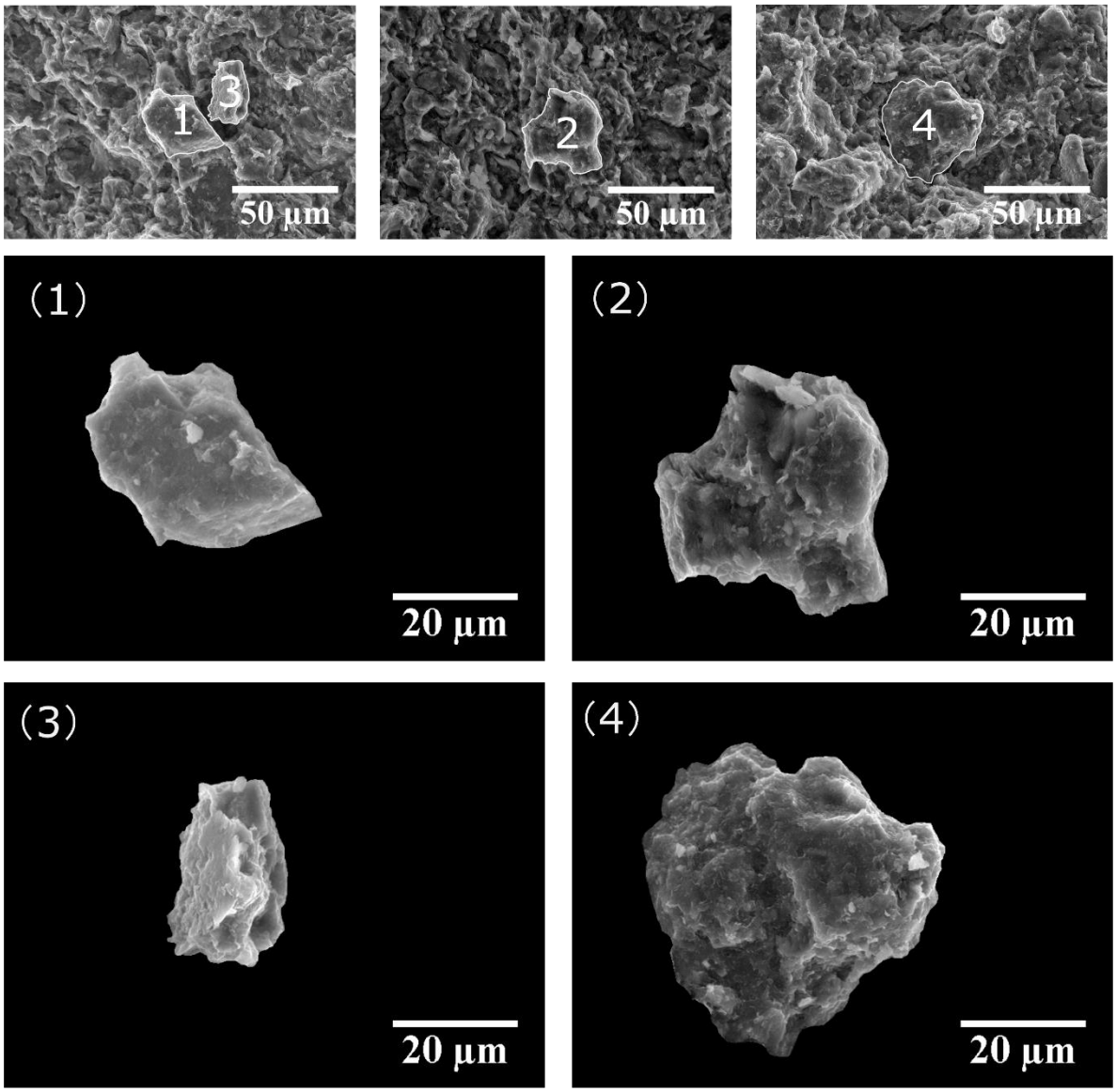

Figure 14: Aggregates of the initial dry density 1.9 g/cm^3 samples selected for calculation of volume strain.

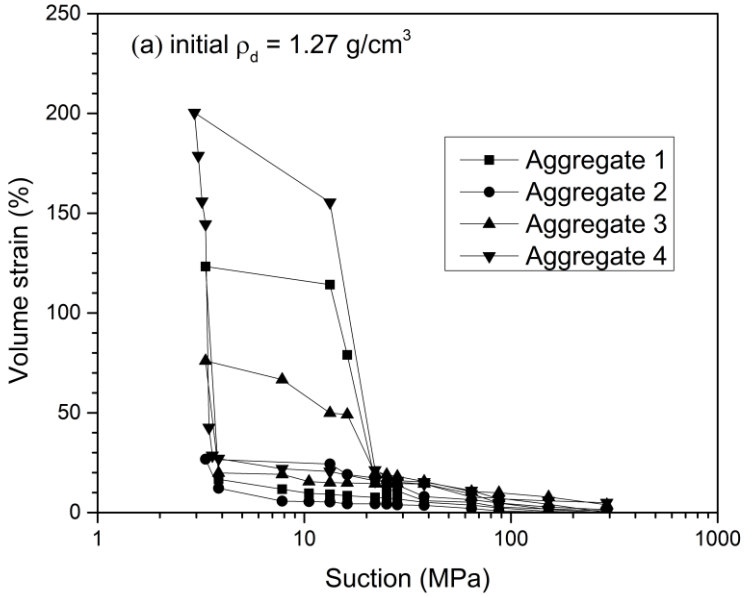

1

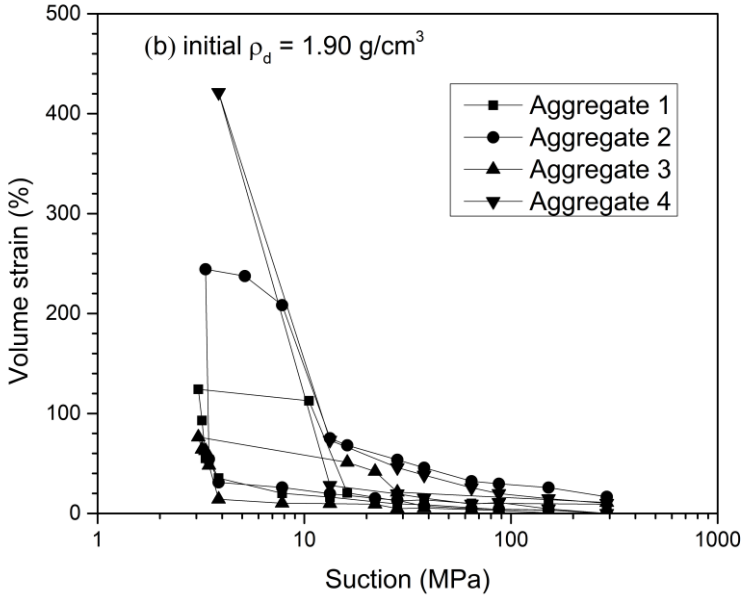

2

3 *Figure 15: Volume strain versus suction for compacted bentonite along wetting and drying*
4 *paths.*

5

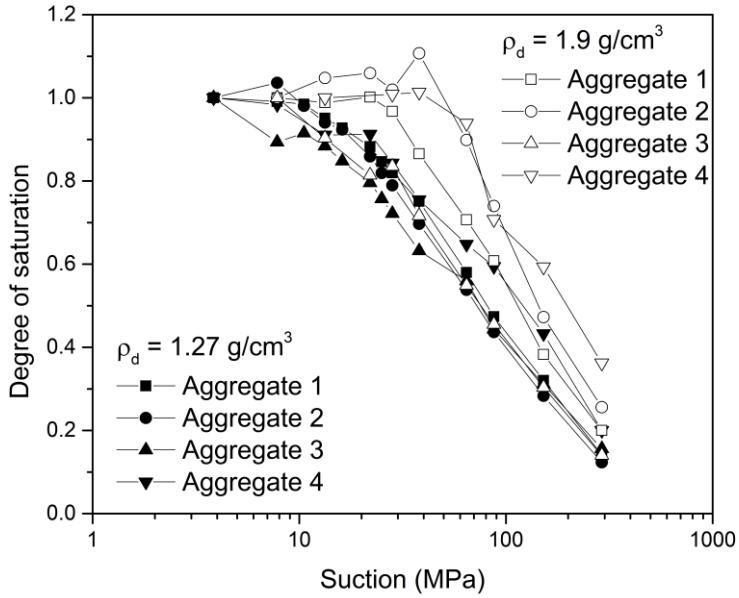

Figure 16: Degree of saturation of aggregates during wetting evaluated from combination of ESEM and WRC measurements.